THERMO-HYDRAULIC COUPLED SIMULATION OF IMMISCIBLE CO_2 FLOODING

ZHAO, C. L.[1,2] – GUO, P.[1,*] – LONG, F.[1]

[1]*State Key Laboratory of Oil and Gas Reservoir Geology and Exploitation, Southwest Petroleum University, Chengdu, China*

[2]*School of Science, Southwest Petroleum University, Chengdu, China*

**Corresponding author*
e-mail: guopingswpi@vip.sina.com

(Received 15th Sep 2018; accepted 12th Nov 2018)

Abstract. As an efficient way to reduce CO_2 in the atmosphere and to extract more hydrocarbons from reservoir, CO_2 flooding is important to reduce environmental and ecological damage by traditional energy. Study on performance of CO_2 in the reservoir and its impact on formation fluids is necessary to oil recovery and to further carbon capture and storage (CCS). In practical, CO_2 is injected into reservoir at low temperature, and both field tests and predictions show that temperature of CO_2 would be lower than that of reservoir while it reaches the target formation, especially for high injection rate. Therefore, further estimation should be conducted to predict how reservoir temperature and properties of fluids are changed during cold CO_2 flooding. In this paper, a mathematical model for non-isothermal immiscible CO_2 flooding is firstly established, then full thermo-hydraulic coupling of the model is simulated on COMSOL by introducing several temperature-dependent and pressure-dependent physical properties of CO_2, oil and rock. The basic reservoir parameters of the model are obtained from one block of Daqing Oilfield, China. Furtherly, effect of CO_2 injection temperature, of CO_2 injection rate and of injector shut-in on reservoir performance is studied. Results show that injection of colder CO_2 causes rapid reduction in reservoir temperature near the injector at the earlier stage. Effect of temperature change is timely shown on physical properties of fluids for full thermo-hydraulic coupling. Oil production rate, oil recovery and production gas-oil ratio all increase as injection temperature increases. Based on a practical situation, this study gives an insight into reservoir performance during cold CO_2 flooding with a numerical method, and it can provide some support for study on temperature change in the reservoir.
Keywords: *immiscible CO_2 EOR, heavy oil, thermo-hydraulic, heat transfer, numerical simulation*

Introduction

Nowadays, settlement of contradiction between environmental protection and growing energy demand is the key to sustainable and high-level development in the future (Ghafoori, et al., 2017; Li, et al., 2017). Although great breakthroughs in green and new energy resources have been continuously achieved, traditional energy like petroleum still dominates the structure. During CO_2 flooding, CO_2 can be stored in the formation for long time after enhancing hydrocarbon recovery, so greenhouse gas emission can be reduced (Zhao, et al., 2014).

In general, temperature contrast between injected CO_2 and oil reservoir is neglected (Smith and Woods, 2011), so it is assumed that oil reservoir is in isothermal situation during injection of CO_2 (Han, et al., 2010). In fact, CO_2 is generally transported and injected at low temperature. For oil reservoir 1500~2000 m below the surface, although CO_2 is in supercritical state at the well bottom after adsorbing heat from formation, it can still be 30~50 K lower than the formation (Li, et al., 2017; Lu and Connell, 2008). A colder region is formed near the injection well (Smith and Woods, 2011). For this temperature contrast, heat transfer happens between CO_2 and formation rock as well as other fluids.

http://www.aloki.hu ● ISSN 1589 1623 (Print) ● ISSN 1785 0037 (Online)
DOI: http://dx.doi.org/10.15666/aeer/1701_409425

Although a large number of numerical simulations have been focused on temperature change during CO_2 injection, they are mainly about CO_2 geological storage (Li and Laloui, 2016; Shabani and Vilcáez, 2018; Zhang, et al., 2015). Meanwhile, some important physical properties of fluids are assumed as constant in most mathematical models for non-isothermal CO_2 flooding (Binshan, et al., 2012; Elyasi, et al., 2016).

In this paper, physical properties of CO_2, oil viscosity, oil density and CO_2 solubility in oil are considered dependent on temperature and pressure. In this way, thermo-hydraulic coupling during CO_2 flooding is effectively achieved. Then change of phase saturation and reservoir temperature is studied by solving the foregoing model in the COMSOL. Finally, we discuss the effect of CO_2 injection temperature and rate on reservoir performance, and how reservoir behaves after injector being shut down.

Materials and methods

Although miscible CO_2 EOR has high displacement efficiency, CO_2 EOR in some reservoirs can not reach the miscible state for formation conditions, fluid properties and technical factors, such as heavy oil reservoirs (Dyer and Ali, 1989; Kang, et al., 2013; Tran, et al., 2017; Zhou and Yang, 2017). Even so, immiscible CO_2 EOR in heavy oil can also obtain desired displacement efficiency by reducing oil viscosity, swelling oil, decreasing oil-gas interfacial tension, vaporizing and extracting light compositions in the oil (Seyyedsar, et al., 2016).

Based on the study Niu (2010), an immiscible CO_2 EOR mass equation for heavy oil, considering solubility of CO_2 in the oil and not considering chemical reaction, has been adopted. Combined with an energy equation, this new CO_2 EOR mathematical model can realize the coupling of temperature field and porous flow. Temperature (T), pressure (p) and saturation (S_o and S_g) are the primary variables.

Assumptions

This model is established on these assumptions: (1) Oil is heavy oil and is treated as one pseudo composition. (2) CO_2 only dissolves in the oil and vaporization of oil into the gas phase is neglected. (3) No mass transfer between the water phase with oil phase or gas phase. (4) The gas phase only contains CO_2 composition, and the water phase only contains water composition. (5) Capillary effect and diffusion effect are not considered. (6) Molar density of every composition in each phase is a constant. When the fluid is injected into the reservoir at a constant volumetric flow rate, volume of composition i changes for mass transfer between oil and gas phases. This is a common phenomenon in the oil reservoir development by gas injection. For different gas and different displacing pressure, its effect varies. Under relatively low pressure, volumetric flow rate $\overrightarrow{u_j}$ of the fluid changes a lot for the dissolution of CO_2 in oil, while, under high pressure, volume of the CO_2 has slight difference before and after dissolving in oil. So the volumetric flow rate $\overrightarrow{u_j}$ of the fluid is assumed as a constant during CO_2 flooding in this study.

Mass equation

Firstly, molar density of component i in phase α is given in *Equation 1:*

http://www.aloki.hu ● ISSN 1589 1623 (Print) ● ISSN 1785 0037 (Online)
DOI: http://dx.doi.org/10.15666/aeer/1701_409425

$$\xi_{i\alpha} = \rho_{i\alpha} / W_i \tag{Eq.1}$$

Then molar density of phase α is shown in *Equation 2:*

$$\xi_\alpha = \sum_{i=1}^{Nc} \xi_{i\alpha} \tag{Eq.2}$$

So molar fraction of component i in phase α is calculated by *Equations 3* and *4:*

$$x_{i\alpha} = \frac{\xi_{i\alpha}}{\xi_\alpha}, \quad i = 1, \quad 2\ldots\ldots N_c \tag{Eq.3}$$

$$\sum_{i=1}^{Nc} x_{io} = 1, \quad \sum_{i=1}^{Nc} x_{ig} = 1 \tag{Eq.4}$$

where $\xi_{i\alpha}$ is molar density of component i in phase α, mol/m^3; ξ_α is molar density of phase α, mol/m^3; $\rho_{i\alpha}$ is mass density of component i in phase α, kg/m^3; W_i is molar mass of component i, kg/mol; $x_{i\alpha}$ is molar fraction of component i in phase α, fraction. The subscript α represents gas phase (g), oil phase (o), and water phase (w); subscripts i represents compositions CO_2 (1), oil (2) and water (3), respectively.

Immiscible CO_2 flooding flow equation which considers CO_2 dissolution in oil can be given as *Equation 5:*

$$\begin{aligned} \frac{\partial}{\partial t}[\phi(S_g\xi_g + S_o\xi_o x_{1o})] + \nabla\cdot(\xi_g\overrightarrow{u_g} + \xi_o\overrightarrow{u_o}x_{1o}) &= q_1 \\ \frac{\partial}{\partial t}(\phi S_o\xi_o x_{2o}) + \nabla\cdot(\xi_o\overrightarrow{u_o}x_{2o}) &= q_2 \\ \frac{\partial}{\partial t}(\phi S_w\xi_w) + \nabla\cdot(\xi_w\overrightarrow{u_w}) &= q_3 \end{aligned} \tag{Eq.5}$$

where φ is reservoir porosity, fraction; S_α phase saturation, %; $\overrightarrow{u_\alpha}$ is flow velocity of phase α, m/s; ∇ is divergence operator; q_α is source or sink of phase α; x_{1o} and x_{2o} is molar fraction of CO_2 and oil in oil phase respectively, %, $x_{1o} + x_{2o} = 100\%$.

Fraction flow equation is introduced to simplify the model. Firstly, mobility is defined as *Equation 6:*

$$\begin{aligned} \lambda_\alpha &= K_{r\alpha} / \mu_\alpha \\ \lambda &= \sum_{\alpha=w,o,g} \lambda_\alpha \end{aligned} \tag{Eq.6}$$

where λ_α is mobility of phase α, m·s/kg; λ is total mobility, m·s/kg; $K_{r\alpha}$ is relative permeability of phase α, fraction; μ_α is viscosity of phase α, mPa·s.

Then, fraction of phase α is given in *Equations 7* and *8:*

http://www.aloki.hu ● ISSN 1589 1623 (Print) ● ISSN 1785 0037 (Online)
DOI: http://dx.doi.org/10.15666/aeer/1701_409425

$$f_\alpha = \frac{\lambda_\alpha}{\lambda} \quad \text{(Eq.7)}$$

$$\sum_{\alpha=\mathrm{w,o,g}} f_\alpha = 1 \quad \text{(Eq.8)}$$

Total flow rate $\vec{u}$ can be expressed as *Equation 9:*

$$\vec{u} = \sum_{\alpha=\mathrm{w,o,g}} \overrightarrow{u_\alpha} \quad \text{(Eq.9)}$$

Then (*Eq. 10*),

$$\nabla \cdot \vec{u} = \sum_{\alpha=\mathrm{w,o,g}} \nabla \cdot \overrightarrow{u_\alpha} \quad \text{(Eq.10)}$$

Capillary pressure is not considered, so pressure of all the phases is the same, expresses as *p*. Flow rate of each phase is shown in *Equation 11:*

$$\begin{aligned} \overrightarrow{u_\mathrm{w}} &= -\frac{\overrightarrow{K}K_\mathrm{rw}}{\mu_\mathrm{w}}(\nabla p - \rho_\mathrm{w}\mathrm{g}\nabla Z) \\ \overrightarrow{u_\mathrm{o}} &= -\frac{\overrightarrow{K}K_\mathrm{ro}}{\mu_\mathrm{o}}(\nabla p - \rho_\mathrm{o}\mathrm{g}\nabla Z) \\ \overrightarrow{u_\mathrm{g}} &= -\frac{\overrightarrow{K}K_\mathrm{rg}}{\mu_\mathrm{g}}(\nabla p - \rho_\mathrm{g}\mathrm{g}\nabla Z) \end{aligned} \quad \text{(Eq.11)}$$

where $\overrightarrow{K}$ is intrinsic permeability tensor, mD; p is pressure, MPa; Z is vertical depth, m; g is gravitational acceleration, m/s^2; ρ_α is density of phase α, kg/m^3.

Relationship of flow rate of each phase and the total one is determined by *Equations 12–14:*

$$\overrightarrow{u_\mathrm{w}} = f_\mathrm{w}\vec{u} \quad \text{(Eq.12)}$$

$$\overrightarrow{u_\mathrm{o}} = f_\mathrm{o}\vec{u} \quad \text{(Eq.13)}$$

$$\overrightarrow{u_\mathrm{g}} = f_\mathrm{g}\vec{u} \quad \text{(Eq.14)}$$

Volumetric fraction of composition *i* in phase α can be given as *Equation 15:*

$$c_{i\alpha} = \frac{x_{i\alpha} / \xi_{i\alpha}}{\sum_{i=1}^{Nc} x_{i\alpha} / \xi_{i\alpha}} \quad \text{(Eq.15)}$$

http://www.aloki.hu ● ISSN 1589 1623 (Print) ● ISSN 1785 0037 (Online)
DOI: http://dx.doi.org/10.15666/aeer/1701_409425

$c_{i\alpha}$ is volumetric fraction of composition *i* in phase *α*, fraction; N_c is number of compositions in the system.

Molar density of phase *α* is defined as *Equation 16:*

$$\xi_\alpha = (\sum_{i=1}^{Nc} x_{i\alpha} / \xi_{i\alpha})^{-1} \quad \text{(Eq.16)}$$

Combining *Equations 15* and *16*, molar density meets the condition given in *Equation 17:*

$$\xi_{i\alpha} c_{i\alpha} = \xi_\alpha x_{i\alpha} \quad \text{(Eq.17)}$$

Molar density of each composition in the system is assumed to be constant, so it can be written as *Equation 18:*

$$\begin{gathered} \xi_{1o} = \xi_{1g} = \xi_1 \\ \xi_{2o} = \xi_2 \\ \xi_{3w} = \xi_3 \end{gathered} \quad \text{(Eq.18)}$$

Without source or sink, substitution of *Equation 18* into *Equation 5*, mass conservation equations are shown in *Equation 19:*

$$\begin{gathered} \frac{\partial}{\partial t}[\phi(S_g + c_{1o} S_o)] + \nabla \cdot [\vec{u}(f_g + c_{1o} f_o)] = 0 \\ \frac{\partial}{\partial t}[\phi(1 - c_{1o}) S_o] + \nabla \cdot [\vec{u}(1 - c_{1o}) f_o] = 0 \\ \frac{\partial}{\partial t}(\phi S_w) + \nabla \cdot (\vec{u} f_w) = 0 \end{gathered} \quad \text{(Eq.19)}$$

Combining the equations in *Equation 19*, pressure equation can be obtained by *Equation 20:*

$$\nabla \cdot [(\frac{\vec{K}K_{ro}}{\mu_o} + \frac{\vec{K}K_{rg}}{\mu_g} + \frac{\vec{K}K_{rw}}{\mu_w}) \cdot \nabla p] = 0 \quad \text{(Eq.20)}$$

$K_{r\alpha}$ is determined by *Equation 21:*

$$K_{r\alpha} = S_\alpha^{\ 2} \quad \text{(Eq.21)}$$

Energy equation

Energy equation of three phase flow during immiscible CO_2 EOR is shown in *Equation 22:*

http://www.aloki.hu ● ISSN 1589 1623 (Print) ● ISSN 1785 0037 (Online)
DOI: http://dx.doi.org/10.15666/aeer/1701_409425

$$\frac{\partial}{\partial t}\left\{[\phi(S_{\mathrm{o}}\rho_{\mathrm{o}}C_{\mathrm{po}}+S_{\mathrm{g}}\rho_{\mathrm{g}}C_{\mathrm{pg}}+S_{\mathrm{w}}\rho_{\mathrm{w}}C_{\mathrm{pw}})+(1-\phi)\rho_{\mathrm{s}}C_{\mathrm{ps}}]T\right\}+$$
$$(\vec{u}_{\mathrm{o}}\rho_{\mathrm{o}}C_{\mathrm{po}}+\vec{u}_{\mathrm{g}}\rho_{\mathrm{g}}C_{\mathrm{pg}}+\vec{u}_{\mathrm{w}}\rho_{\mathrm{w}}C_{\mathrm{pw}})\cdot\nabla \mathrm{T}= \quad \text{(Eq.22)}$$
$$\nabla\cdot\left\{[\phi(S_{\mathrm{o}}k_{\mathrm{o}}+S_{\mathrm{g}}k_{\mathrm{g}}+S_{\mathrm{w}}k_{\mathrm{w}})+(1-\phi)k_{\mathrm{s}}]\nabla T\right\}+(\phi Q_{\mathrm{f}}+(1-\phi)Q_{\mathrm{s}})$$

in which, T is the temperature, K; $C_{\mathrm{p}\alpha}$ is the constant pressure heat capacity of phase α, J/(kg·K); k_{α} is the thermal conductivity of phase α, W/(m·K); k_{e} is the effective thermal conductivity of reservoir, W/(m·K); k_{s} is the thermal conductivity of rock in the reservoir, W/(m·K); Q_T is the source or sink of heat in the system, W; Q_{f} and Q_{s} are the source or sink of heat in fluid and rock respectively, W.

Auxiliary equations

Saturation constraint equation is given in *Equation 23:*

$$S_{\mathrm{o}}+S_{\mathrm{w}}+S_{\mathrm{g}}=1 \quad \text{(Eq.23)}$$

Physical properties

In this paper, CO_2 property parameters (density, viscosity, heat capacity and thermal conductivity) are based on the America National Institute of Standards and Technology NIST online database.

Compared with heat capacity and thermal conductivity of CO_2, those of oil change a little with temperature and pressure under reservoir condition, and are set to 0.15 W/(m·K) and 2100.00 J/(kg·K) in this study, respectively. CO_2 solubility in heavy oil is calculated by the correlation developed by Chung et al. (1988), as shown in *Equation 24:*

$$R_{\mathrm{s}}=\frac{0.178094}{A_1\gamma^{A_2}(1.8T-459.67)^{A_7}+A_3(1.8T-459.67)^{A_4}\,\mathrm{e}^{[-145.0377A_5p+A_6/(145.0377p)]}} \quad \text{(Eq.24)}$$

where R_{s} is solubility of CO_2 in oil, m^3/m^3; A_1, A_2, A_3, A_4, A_5, A_6, A_7 are empirical parameters, 0.004934, 4.092, 5.71×10^{-7}, 1.6428, 6.763×10^{-4}, 781.334 and -0.2499, respectively; γ is relative density of oil, and is set to 0.808 in the paper. Viscosity of CO_2-oil system is given by the equation proposed by Lederer (1933) for CO_2 flooding of heavy oil, as given in *Equation 25:*

$$\ln\mu_{\mathrm{m}}=x_{1\mathrm{o}}\ln(\mu_{\mathrm{g}})+x_{2\mathrm{o}}\ln(\mu_{\mathrm{o}}) \quad \text{(Eq.25)}$$

where μ_{m} is viscosity of CO_2-oil system, mPa·s. Welker and Dunlop (1963) presented correlation between oil swelling factor and solubility of CO_2 in oil, as shown in *Equation 26:*

$$F_{\mathrm{s}}=1+6.233\times10^{-5}R_{\mathrm{s}} \quad \text{(Eq.26)}$$

http://www.aloki.hu ● ISSN 1589 1623 (Print) ● ISSN 1785 0037 (Online)
DOI: http://dx.doi.org/10.15666/aeer/1701_409425

where F_s, is swelling factor of oil. Density of heavy CO_2-oil system is calculated by the equation presented by Quail et al. (1988), as given in *Equation 27:*

$$\rho = [B_1 - B_2 T + B_3 p_s] \frac{e^{(-B_4 x_{1o})}}{1 + B_5 x_{CH_4}} \quad \text{(Eq.27)}$$

where p_s is saturation pressure of oil, MPa; B_1, B_2, B_3, B_4 and B_5 are empirical parameters, 1.1571, 6.534×10^4, 7.989×10^4, 3.58×10^3, 0.05086; x_{CH_4} is molar fraction of CH_4 in oil, %.

In this paper, compressibility of rock is not considered, so its density is a constant. Density of rock is 2640 kg/m^3. Isobaric heat capacity of rock is slightly affected by temperature (Eppelbaum, et al., 2014), so it is a constant in this paper 850.00 J/(kg·K). Correlation of thermal conductivity of sandstone with temperature adopts the one established by Kutas (1977), as given in *Equation 28:*

$$k_s = k_{20} - (k_{20} - 1.38072)[\exp(0.725 \frac{T - 293.15}{T - 143.15}) - 1] \quad \text{(Eq.28)}$$

where k_{20} is thermal conductivity of rock at 293.15 K, W/(m·K), 3.00 W/(m·K) in this paper; k_s is thermal conductivity of rock at given temperature T, W/(m·K).

Geological model

During CO_2 flow in oil reservoir from the injector to the producer, CO_2 displaces oil ahead (*Fig. 1*), and temperature decreases in the reservoir especially around the injector. An inverted five-spot well pattern is made to perform the CO_2 flooding, as shown in *Figure 2*. Size of the injection-production unit is 144 m × 144 m × 8.3 m (well injector-producer spacing: 100 m). To simulate temperature change in the reservoir more correctly, the model considers heat transfer between reservoir and baserock or caprock. Other input reservoir and CO_2 injection data used in the simulation can be found in *Table 1*, of which the basic parameters of the reservoir are obtained from one block of Daqing Oilfield, China.

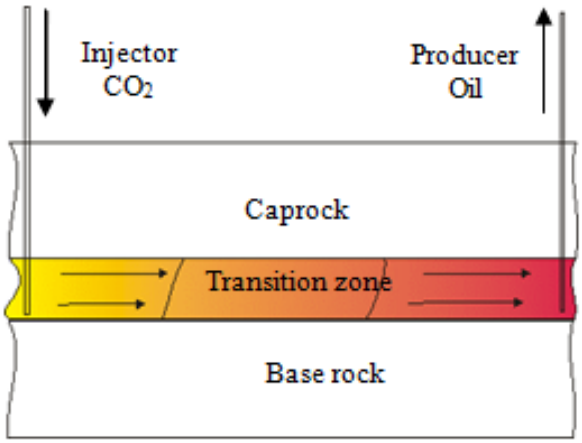

Figure 1. *Scheme of CO_2 injection profile in the reservoir*

http://www.aloki.hu ● ISSN 1589 1623 (Print) ● ISSN 1785 0037 (Online)
DOI: http://dx.doi.org/10.15666/aeer/1701_409425

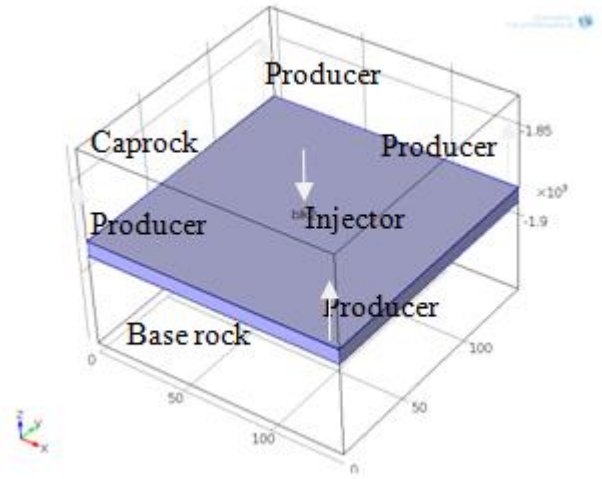

Figure 2. *Scheme of inverted five-spot well pattern in the COMSOL*

Table 1. *Input parameters of non-isothermal CO_2 EOR simulation in inverted five-spot well pattern*

Initial formation pressure, MPa	20.50	Oil density in reservoir, kg/m^3	808.80
Average pressure gradient, MPa/100 m	1.12	Oil viscosity in reservoir, mPa·s	2.86
Reservoir temperature, K	358.15	S_{oi}, %	56.60
Average geothermal gradient, K/100 m	4.72	S_{wi}, %	43.40
Middle depth, m	1880.00	Residual oil saturation after CO_2 flooding S_{or}, %	23.30
Fracture	No	Water saturation after CO_2 flooding S_{wr}, %	40.00
Porosity, %	12.30	Gas saturation after CO_2 flooding S_{gr}, %	36.70
K, mD	1.28	Injector-producer spacing, m	100.00
Average sand thickness, m	8.30	CO_2 injection rate, t/d	5

Results and discussion

Base case

This mathematical model is solved on PDE module of COMSOL, and initial and boundary conditions can be customized on this software. Firstly, base case is simulated with input data shown in *Table 1* for 10 years, to study distribution of oil and gas saturation as well as temperature in the reservoir under continuous injection of CO_2.

Variations of phase saturation (S_g and S_o) distribution in the reservoir

Areal distribution of CO_2 saturation S_g and oil saturation S_o after 0.5 a and 10 a of CO_2 injection are shown in *Figures 3* and *4*, respectively. From these figures, oil is flooded out with continuous injection of CO_2, increasing CO_2 saturation and decreasing oil saturation. The flooding front of CO_2 is not a uniform face, but a flooding transition district which keeps expanding towards the injector.

http://www.aloki.hu ● ISSN 1589 1623 (Print) ● ISSN 1785 0037 (Online)
DOI: http://dx.doi.org/10.15666/aeer/1701_409425

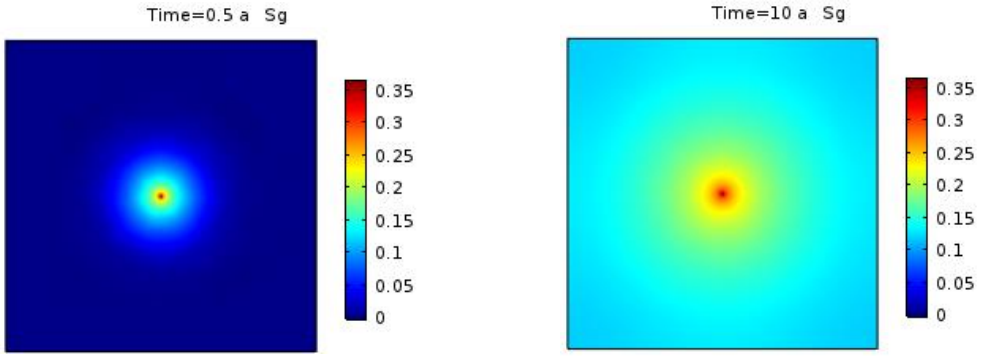

Figure 3. *Areal distribution of S_g at (a) 0.5 a, (b) 10 a*

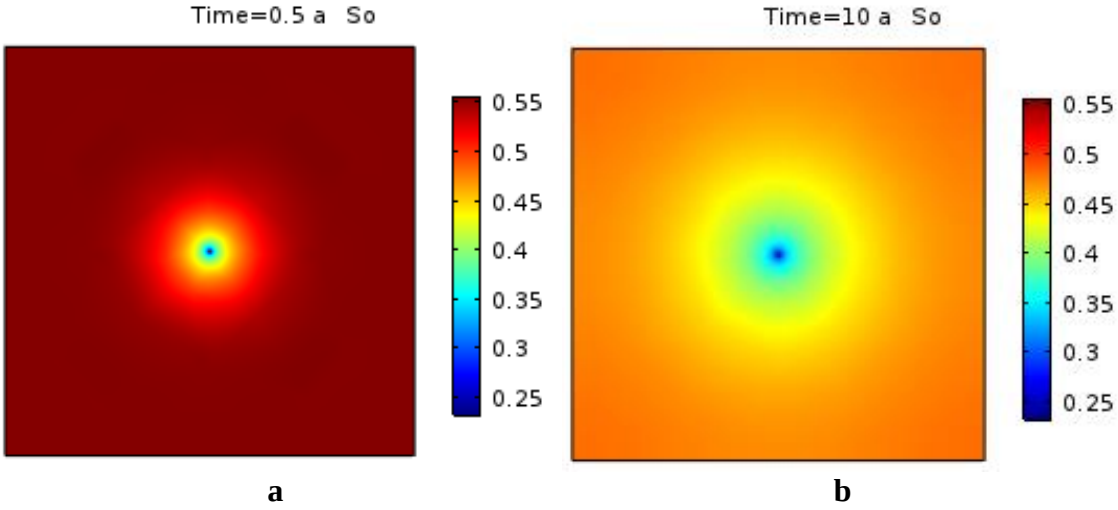

Figure 4. *Areal distribution of S_o at (a) 0.5 a, (b) 10 a*

To quantify CO_2 and oil saturation during CO_2 injection, S_g and S_o along the injector-producer line after 0.5 a, 2.5 a, 5 a, 7.5 a, and 10 a injection of CO_2 are obtained in *Figure 5*.

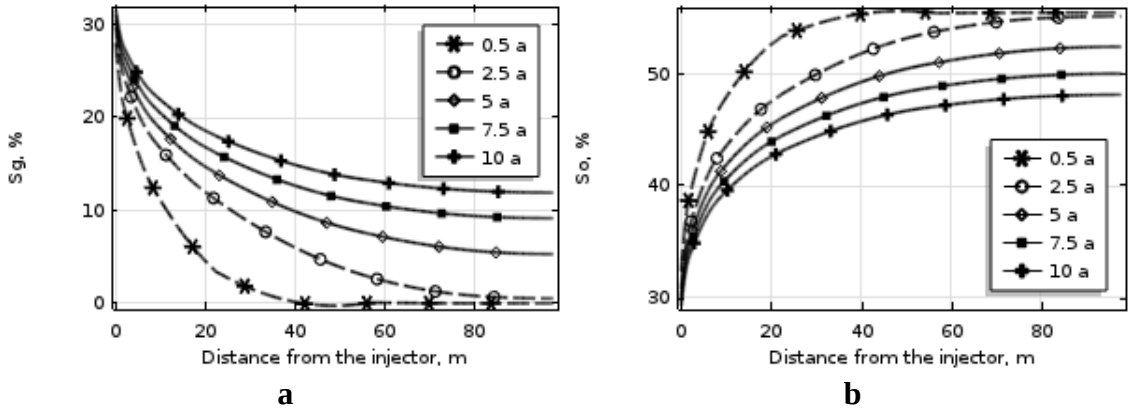

Figure 5. *S_g and S_o distributions along the injector-producer line at various times*

http://www.aloki.hu ● ISSN 1589 1623 (Print) ● ISSN 1785 0037 (Online)
DOI: http://dx.doi.org/10.15666/aeer/1701_409425

At the earlier stage (0-2.5 a), large amount of oil is displaced out by CO_2 to the producers, so S_o is decreased quickly near the injector and S_g is increased instead. CO_2 does not break through, and no CO_2 is produced at the producer. For its high saturation, oil still dominates fluids flow in the reservoir. After CO_2 injection for 2.5 a, CO_2 starts to break through in the producer, and it forms a continuous phase in the reservoir. S_o is decreased in the whole reservoir. Although CO_2 can be dissolved in the oil with certain amount, most CO_2 flows in the reservoir as free gas. Compared with oil viscosity, viscosity of CO_2 is very low, so unfavorable mobility ratio is formed in CO_2 flooding. This reduces flow capacity of oil and displacement efficiency. As time goes on, reduction in oil saturation at the same point on the injector-producer line gradually decreases for the same time gap.

Figure 6 shows distribution of flow velocity of CO_2 u_g and oil u_o at the earlier stage (0.5 a) and end (10 a) of CO_2 injection. Direction and quantity of phase velocity are represented by direction and size of the arrows, respectively. The arrow is larger, the velocity is higher. For both phases, velocity on the injector-producer line is the largest velocity among the points on circle around the injector. It gradually decreases away from line on the same circle. At the earlier stage, CO_2 just flows around the injector, while oil is the continuous phase, covering the whole oil reservoir. The point is closer to the injector, u_g is larger. u_o has a reverse changing rule. As CO_2 flooding continuing, more CO_2 is injected into the reservoir, and oil near the injector is flooded towards the producer. S_o in this area reduces, so does its flowing ability. For the expansion of CO_2 in the reservoir, CO_2 on the injector-producer line breaks through in the producer at certain time. Then it forms a continuous phase. Since then, flow resistance of oil increasingly growing, and its relative permeability decreases. This is not favorable for the displacement of oil.

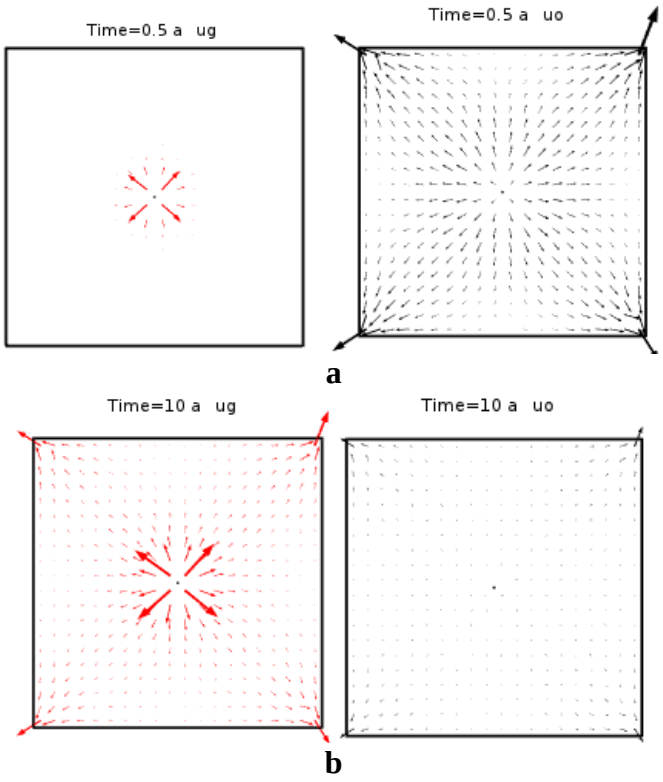

Figure 6. *u_g and u_o distribution at (a) 0.5 a and (b) 10 a*

http://www.aloki.hu ● ISSN 1589 1623 (Print) ● ISSN 1785 0037 (Online)
DOI: http://dx.doi.org/10.15666/aeer/1701_409425

Variations of reservoir temperature (T) distribution in the reservoir

Areal distribution of *T* during injection of CO_2 at 303.15 K for different times is shown in *Figure 7*. *T* along the injector-producer line is also drawn, as shown in *Figure 8*. From *Figures 7* and *8*, injection of colder CO_2 at the earlier stage causes rapid reduction in *T* near the injector. As injection continues, change in *T* slows down, and temperature gradually reaches a stable state after certain time.

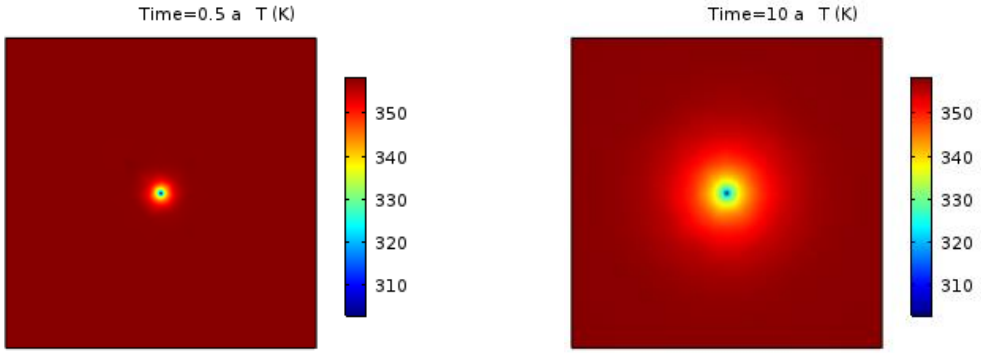

Figure 7. *Areal distribution of T at (a) 0.5 a, (b) 10 a*

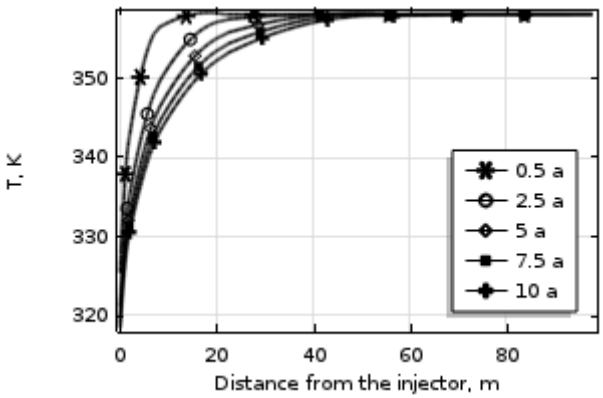

Figure 8. *Variation of T along the injector-producer line*

From temperature profile along the injector-producer line, as shown in *Figure 9*, we can clearly see that temperature contour line is not vertical, but arc-shaped. As shown in *Figure 10*, after CO_2 is injected into the reservoir at temperature T_{inj} lower than the formation one (T_0), there is a temperature contrast (thermal gradient) between CO_2 and formation. Temperature of CO_2 gradually is increased for heat adsorption from the formation as flowing deep into the reservoir. Formation temperature near the injector is decreased for continuously injected cold CO_2 at the same time. Then, heat in the caprock and base rock is transferred into the oil reservoir timely to offset the temperature drop in formation to some extent. Therefore, temperature changes more quickly in the middle of oil reservoir than that upper or lower zone.

Although fresh CO_2 is continuously injected into the reservoir, it has limited effect on temperature of the whole field. Even so, physical properties and flow conditions

http://www.aloki.hu ● ISSN 1589 1623 (Print) ● ISSN 1785 0037 (Online)
DOI: http://dx.doi.org/10.15666/aeer/1701_409425

change a lot in the near-wellbore area, so temperature change still has some effect on the CO_2 displacement efficiency.

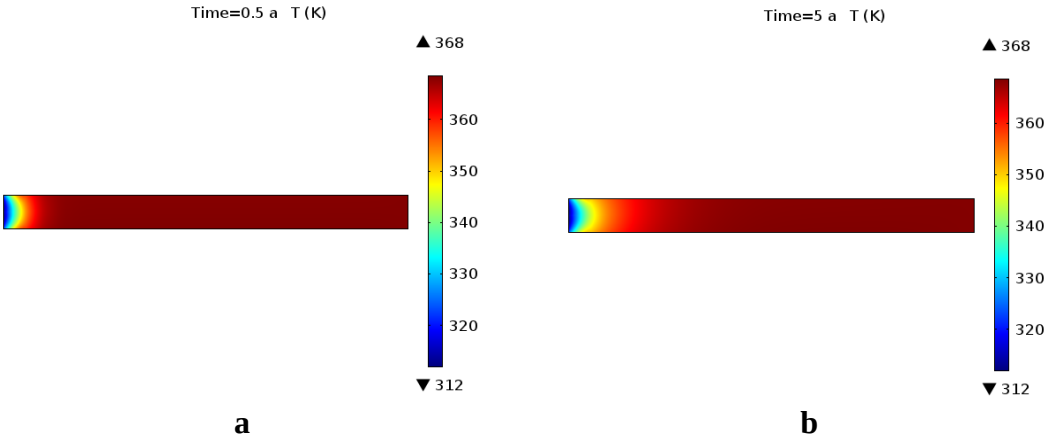

Figure 9. *Reservoir temperature (T) profile along the injector-producer line at (a) 0.5 a and (b) 5 a*

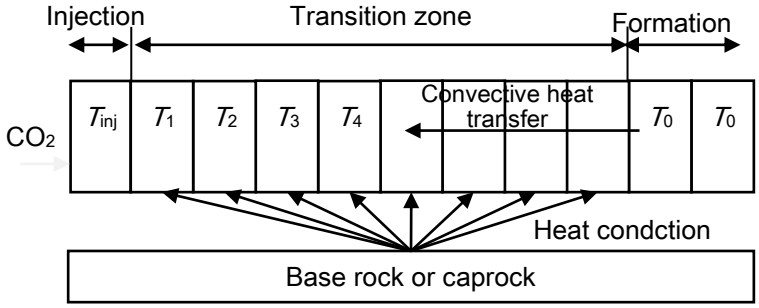

Figure 10. *Scheme of heat transfer in the reservoir during low temperature CO_2 injection*

Production performance

Oil production rate and production gas-oil ratio (GOR) of different CO_2 injection time are shown in *Figure 11*. It is shown that at the first stage of immiscible CO_2 flooding, there is a slight increase in oil production, and no CO_2 is produced. Then oil production is reduced rapidly and GOR is increased at the same time. At the end of CO_2 injection, oil production is only one third of its maximum and GOR is 50 m^3/m^3. At beginning, large flowing resistance should be overcome by CO_2 to displace out oil in the pore, and distribution of oil, water and CO_2 in the reservoir are changed quickly. As injection continues, flow condition in the near-wellbore areas is improved to some extent, so does oil production. At 2.5 a, CO_2 starts to breakthrough in the producer and it forms a continuous phase in the formation. Therefore, previous continuous oil is cut into oil droplets or oil threads in some areas, unfavorable for oil flow in the reservoir. CO_2 cannot get miscible with oil in immiscible flooding, and huge viscosity contrast can form unfavorable mobility ratio. As more CO_2 is injected, its flowing resistance is reduced furtherly and more CO_2 is produced from the producer.

http://www.aloki.hu ● ISSN 1589 1623 (Print) ● ISSN 1785 0037 (Online)
DOI: http://dx.doi.org/10.15666/aeer/1701_409425

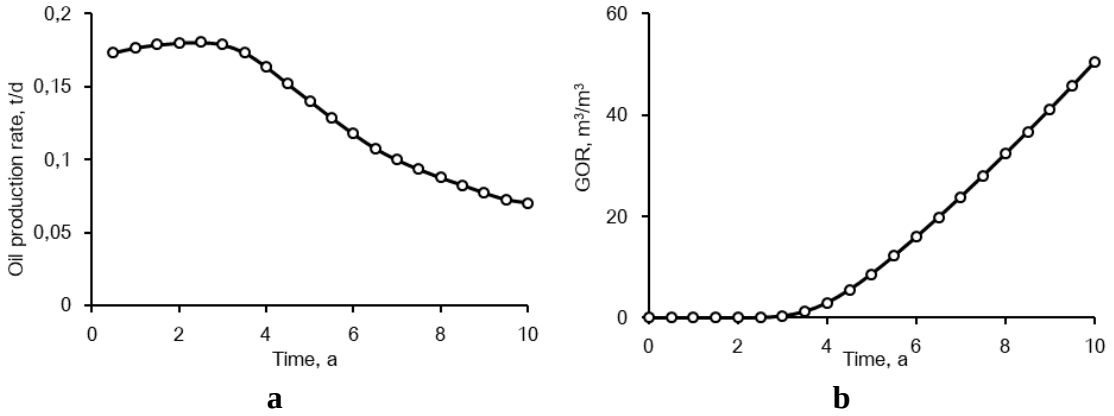

a **b**

Figure 11. *(a) Oil production rate and (b) GOR of five-spot pattern for continuous CO_2 injection*

As shown in *Figure 12,* oil recovery increases quickly before CO_2 breakthrough, and grows more slowly thereafter. In this simulation, permeability of the reservoir is extremely low and no fracture is introduced to the model. So producing degree of oil is relatively low. Oil recovery by CO_2 flooding is only about 5% at the end of production.

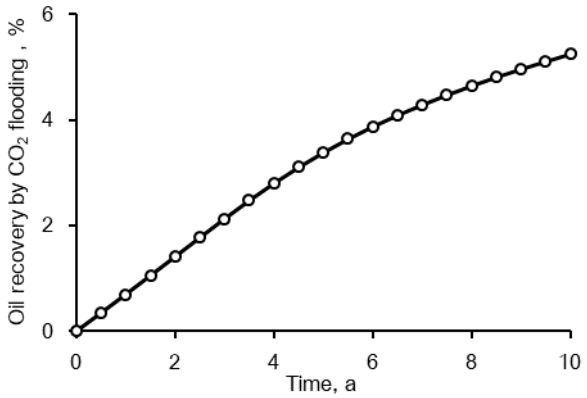

Figure 12. *Oil recovery by CO_2 flooding vs time for continuous CO_2 injection*

Sensitivity analysis

Effect of CO_2 injection temperature on reservoir behavior

Oil production, GOR and oil recovery during CO_2 injection for CO_2 injection temperature of 303.15 K, 323.15 K and 343.15 K are shown in *Figures 13* and *14*, respectively. As shown in these figures, higher the CO_2 injection temperature, more oil is produced. Under low temperature, oil viscosity, oil density and CO_2 viscosity are increased to some degree in the colder area near the injector, which is not favorable for displacement efficiency of oil by CO_2. CO_2 injection temperature is higher, and the density and viscosity of oil in the near-wellbore area is lower. Under higher temperature, oil can flow more easily, and flowing condition of oil and gas in this area is improved. Oil production, oil recovery and GOR are higher. Therefore, increase in CO_2 injection temperature can reduce the unfavorable effect of injected CO_2 on fluid

http://www.aloki.hu ● ISSN 1589 1623 (Print) ● ISSN 1785 0037 (Online)
DOI: http://dx.doi.org/10.15666/aeer/1701_409425

flowing capacity in the area around the injector, so more oil displacement efficiency can be achieved.

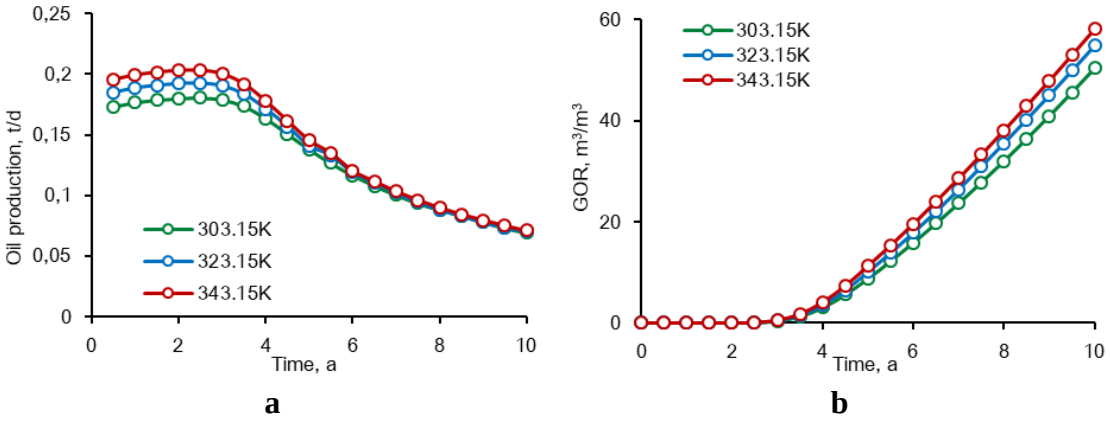

Figure 13. *(a) Oil production and (b) GOR with different CO_2 injection temperature*

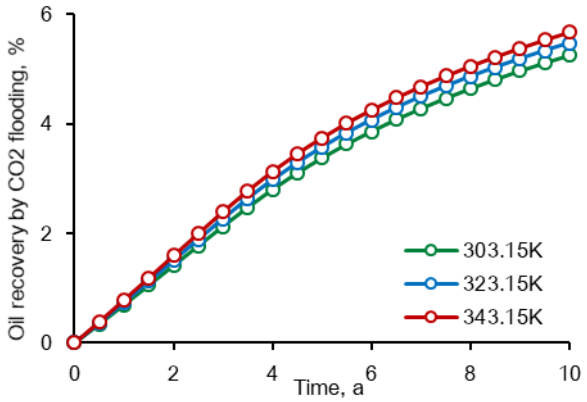

Figure 14. *Oil recovery by CO_2 flooding vs time with different CO_2 injection temperature*

Effect of CO_2 injection rate on reservoir behavior

Oil production, GOR and oil recovery under different CO_2 injection rate (5.00 t/d, 10.00 t/d and 15.00 t/d) are compared in *Figure 15*. In *Figure 19*, oil production is higher for larger CO_2 injection rate, while there is no big difference in oil production after CO_2 breakthrough. As shown in *Figure 15*, much more CO_2 is produced after breakthrough under higher injection rate, so GOR is much higher. Increase in CO_2 injection rate can improve driving force and displacement efficiency of CO_2, and oil recovery is apparently increased (*Fig. 16*).

Comparison

Specific data of reservoir temperature and reservoir performance are extremely dependent on reservoir parameters and injection data, so it is unpractical to compare the particular data with those from other study. While the changing rules are consistent with some similar studies, as in the research by Smith and Woods (2011), a thermal front is formed in the reservoir during injection of cold CO_2 and viscosity and density of CO_2 is

http://www.aloki.hu ● ISSN 1589 1623 (Print) ● ISSN 1785 0037 (Online)
DOI: http://dx.doi.org/10.15666/aeer/1701_409425

increased as its temperature is increased. Moreover, in the 2016 research by Elyasi et al. (2016) shows that temperature change around the injection well can induce thermal strain, which can influence porosity and permeability. More studies show that multi-physical coupling during CO_2 injection exists, and in-depth studies should be focused on this field to obtain high efficiency on CO_2 flooding and CCS. Our ongoing study is also conducted in this direction.

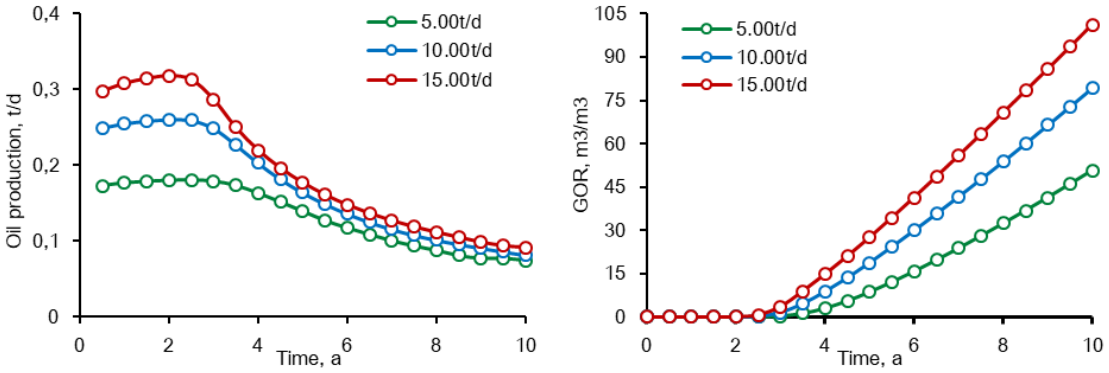

a **b**

Figure 15. *(a) Oil production and (b) GOR with different CO_2 injection rate*

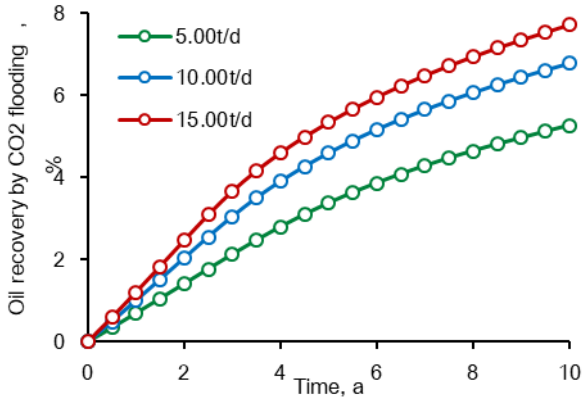

Figure 16. *Oil recovery by CO_2 flooding vs time with different CO_2 injection rate*

Conclusions

An effective method is developed in this paper to study and predict reservoir temperature and reservoir performance during cold CO_2 flooding. A non-isothermal immiscible CO_2 EOR mathematical model for heavy oil is established by introducing temperature-dependent and pressure-dependent parameters of fluids, then this model is solved and simulated by the Finite Element Method based software COMSOL. The results show that properties of fluids in the reservoir, especially near the injector, and reservoir performance can be influenced by the injection of CO_2 under lower temperature than that of reservoir. Based on this research, more numerical simulations on oil development and production, especially multi-physics coupling, can be realized by combining built-in and user-defined models in COMSOL. Moreover, COMSOL can

http://www.aloki.hu ● ISSN 1589 1623 (Print) ● ISSN 1785 0037 (Online)
DOI: http://dx.doi.org/10.15666/aeer/1701_409425

be effectively combined with other software, so more complex pore-scale or reservoir-scale multi-physical simulations can be further realized.

Acknowledgements. This work was financially supported by the Open Fund (PLN201830) of State Key Laboratory of Oil and Gas Reservoir Geology and Exploitation (Southwest Petroleum University).

REFERENCES

[1] Binshan, J., Yu-Shu, W., Jishun, Q., Tailiang, F., Zhiping, L. (2012): Modeling CO_2 miscible flooding for enhanced oil recovery. – Petroleum Science 9: 192-198.
[2] Chung, F. T. H., Jones, R. A., Nguyen, H. T. (1988): Measurements and correlations of the physical properties of CO_2 /heavy-crude-oil mixtures. – SPE Reservoir Engineering 3: 822-828.
[3] Dyer, S. B., Ali, S. M. F. (1989): The potential of the immiscible carbon dioxide flooding process for the recovery of heavy oil. – Technical Meeting/Petroleum Conference of The South Saskatchewan Section. Regina, Saskatchewan, Canada.
[4] Elyasi, A., Goshtasbi, K., Hashemolhosseini, H. (2016): A coupled thermo-hydro-mechanical simulation of reservoir CO_2 enhanced oil recovery. – Energy & Environment 5: 524-541.
[5] Eppelbaum, L., Kutasov, I., Pilchin, A. (2014): Applied Geothermics. – Springer, Berlin Heidelberg, New Delhi.
[6] Ghafoori, M., Tabatabaei-Nejad, S. A., Khodapanah, E. (2017): Modeling rock-fluid interactions due to CO_2 injection into sandstone and carbonate aquifer considering salt precipitation and chemical reactions. – Journal of Natural Gas Science and Engineering 37: 523-538.
[7] Han, W. S., Stillman, G. A., Lu, M., Lu, C. (2010): Evaluation of potential nonisothermal processes and heat transport during CO_2 sequestration. – Journal of Geophysical Research: Solid Earth 115: 1-23.
[8] Kang, S., Gao, C., Zhang, S. (2013): Scientific research and field application of CO_2 immiscible flooding in heavy oil recovery. – SPE Enhanced Oil Recovery Conference. Kuala Lumpur, Malaysia.
[9] Kutas, R. I. (1977): Investigation of heat flow in the territory of the Ukraine. – Tectonophysics 41: 139-145.
[10] Lederer, E. L. (1933): Mischungs- und Verdünnungsviskosität. – World Pet. Cong. 2: 526-528.
[11] Li, C., Laloui, L. (2016): Coupled multiphase thermo-hydro-mechanical analysis of supercritical CO_2 injection: benchmark for the in Salah surface uplift problem. – International Journal of Greenhouse Gas Control 51: 394-408.
[12] Li, X., Li, G., Wang, H., Tian, S., Song, X., Lu, P., Wang, M. (2017): A unified model for wellbore flow and heat transfer in pure CO_2 injection for geological sequestration, EOR and fracturing operations. – International Journal of Greenhouse Gas Control 57: 102-115.
[13] Lu, M., Connell, L. (2008): Non-isothermal flow of carbon dioxide in injection wells during geological storage. – International Journal of Greenhouse Gas Control 2: 248-258.
[14] Niu, B. (2010): CO_2 flooding in chalk reservoirs-experiments with X-ray computed tomography and reactive transport modelling. – PhD Thesis, Technical University of Denmark, pp.27-30.
[15] Quail, B., Hill, G. A., Jha, K. N. (1988): Correlations of viscosity, gas solubility, and density for Saskatchewan heavy oils. – Industrial & Engineering Chemistry Research 27: 519-523.

http://www.aloki.hu ● ISSN 1589 1623 (Print) ● ISSN 1785 0037 (Online)
DOI: http://dx.doi.org/10.15666/aeer/1701_409425

[16] Seyyedsar, S. M., Farzaneh, S. A., Sohrabi, M. (2016): Experimental investigation of tertiary CO_2 injection for enhanced heavy oil recovery. – Journal of Natural Gas Science and Engineering 34: 1205-1214.
[17] Shabani, B., Vilcáez, J. (2018): A fast and robust TOUGH2 module to simulate geological CO_2 storage in saline aquifers. – Computers & Geosciences 111: 58-66.
[18] Smith, W. J. R., Woods, A. W. (2011): Some implications of cold CO_2 injection into deep saline aquifers. – Geophysical Research Letters 38: 1-6.
[19] Tran, T. Q. M. D., Neogi, P., Bai, B. (2017): Stability of CO_2 displacement of an immiscible heavy oil in a reservoir. – SPE Journal 02: 539-547.
[20] Welker, J. R., Dunlop, D. D. (1963): Physical properties of carbonate oils. – Journal of Petroleum Technology 15: 873-875.
[21] Zhang, R., Winterfeld, P. H., Yin, X., Xiong, Y., Wu, Y. (2015): Sequentially coupled THMC model for CO_2 geological sequestration into a 2D heterogeneous saline aquifer. – Journal of Natural Gas Science and Engineering 27: 579-615.
[22] Zhao, D. F., Liao, X. W., Yin, D. D. (2014): Evaluation of CO_2 enhanced oil recovery and sequestration potential in low permeability reservoirs, Yanchang Oilfield, China. – Journal of the Energy Institute 87: 306-313.
[23] Zhou, D., Yang, D. (2017): Scaling criteria for waterflooding and immiscible CO_2 flooding in heavy oil reservoirs. – Journey of Energy Resources Technology 139.

http://www.aloki.hu ● ISSN 1589 1623 (Print) ● ISSN 1785 0037 (Online)
DOI: http://dx.doi.org/10.15666/aeer/1701_409425